

# Flow and heat transfer control over an external surface using a porous block array arrangement

P. C. HUANG and K. VAFAI

Department of Mechanical Engineering, The Ohio State University, Columbus, OH 43210, U.S.A.

(Received 21 September 1992 and in final form 8 March 1993)

**Abstract**—In this study, a composite system made of multiple porous block structure used for flow and heat transfer control will be analyzed. The primary objective of this study is to analyze the changes in the flow pattern and heat transfer characteristics due to the existence of the multiple porous block structure. A general flow model that accounts for the effects of the impermeable boundary and inertial effects is used to describe the flow inside the porous region. Solutions of the problem have been carried out using a finite-difference method through the use of a stream function–vorticity transformation. Various interesting characteristics of the flow and temperature fields in the composite layer are analyzed and discussed in detail. The effects of several governing dimensionless parameters, such as the Darcy number, Reynolds number, Prandtl number, the inertia parameter, as well as the effects of pertinent geometric parameters, are thoroughly explored.

## INTRODUCTION

CONVECTIVE heat transfer in fluid-saturated porous media has gained considerable attention in recent decades due to its relevance in a wide range of applications such as thermal insulation engineering, water movements in geothermal reservoirs, heat pipes, underground spreading of chemical waste, nuclear waste repository, geothermal engineering, grain storage, and enhanced recovery of petroleum reservoirs. Most of the previous studies related to transport through porous media are based on investigating flow through a semi-infinite porous medium or flow through structures which are fully filled with the porous medium. But, due to the difficulties in simultaneously solving the coupled momentum equations for both porous and fluid regions, analysis of the porous/fluid composite structures which occur in a wide variety of practical applications have been mostly ignored.

A general theory and numerical calculation techniques for flow field and heat transfer in recirculating flow without including the porous medium have been developed by Gosman [1], and was successfully used by various investigators such as Gooray *et al.* [2, 3]. They have shown that these methods can be applied to give reasonably accurate quantitative heat transfer results for the separated forced convection behind a backstep. However, to the best of the authors' knowledge, there has not been any investigations on the forced convection over multiple porous blocks.

For an external boundary exposed to a semi-infinite porous medium, Cheng [4] and Bejan [5] have presented closed form results for the local Nusselt number as function of the Peclet number based on Darcy's law. Kaviany [6] has solved a similar problem and obtained Karman–Pohlhausen solutions based on the Brinkman–Forshheimer-extended equation which

accounts for the boundary and inertia effects. Vafai and Thiyagaraja [7] presented a theoretical analysis for a general class of problems involving interface interactions on flow and heat transfer for three different types of interface zones. They obtained analytical solutions for both velocity and temperature distributions as well as the analytical expressions for the Nusselt number for all of these interface conditions. Vafai and Thiyagaraja [7] also presented a detailed theoretical solution for the velocity and temperature fields as well as the Nusselt number distribution for flow over an external boundary embedded in a porous medium. Cheng [8] obtained the temperature distribution for a horizontal cylinder and a sphere placed in a uniform flow through a porous medium, and Cheng and Zheng [9] reported the inertia and thermal dispersion effects on flow and temperature fields for a horizontal line heat source in a porous medium.

While many studies have been performed in these areas, little attention has been focused on porous/fluid composite system. Vafai and Kim [10] have studied numerically the flow and heat transfer over a flat plate with an attached porous substrate. They carried out a fundamental study of the effects of Darcy and Prandtl numbers, inertia parameter, and the ratio of the conductivity of the porous material to that of the fluid. They found that the porous substrate caused the flow to deflect and resulted in a decrease in the frictional drag. They also found that depending on the value of the thermal conductivity of the porous wafer, the substrate can either augment or decrease the heat transfer from the external boundary. However, there is very little work on forced convective flow in more complicated configurations. The present work addresses a fundamental investigation of one such complicated configuration, namely a system composed of intermittent porous blocks.

## NOMENCLATURE

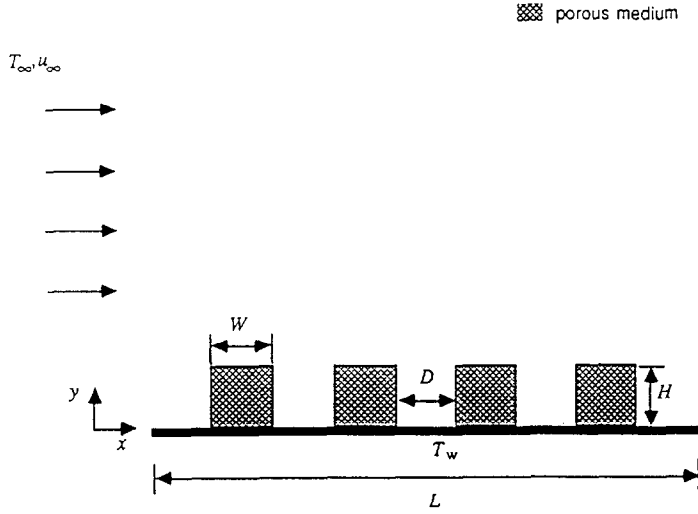
$A$	dimensionless geometric parameter, $W^*/H^*$	$y$	vertical coordinate [m].
$B$	dimensionless geometric parameter, $D^*/H^*$	Greek symbols	
$D$	spacing between blocks [m <sup>-1</sup> ]	$\alpha$	thermal diffusivity [m <sup>2</sup> s <sup>-1</sup> ]
$Da_L$	Darcy number, $K/L^2$	$\Gamma$	general diffusive coefficient, used in equation (16)
$F$	a function used in expressing inertia terms	$\Delta x$	$x$ -direction width of the control volume
$h$	convective heat transfer coefficient [W m <sup>-2</sup> K <sup>-1</sup> ]	$\Delta y$	$y$ -direction width of the control volume
$H$	thickness of the porous block [m]	$\delta x$	$x$ -direction distance between two adjacent grid points
$g(x, y)$	curve defining the porous/fluid interface	$\delta y$	$y$ -direction distance between two adjacent grid points
$k$	thermal conductivity [W m <sup>-1</sup> K <sup>-1</sup> ]	$\epsilon$	porosity of the porous medium
$K$	permeability of the porous medium [m <sup>2</sup> ]	$\theta$	dimensionless temperature, $(T - T_\infty)/(T_w - T_\infty)$
$l_1$	length of plate upstream from the blocks [m]	$\Lambda_L$	inertial parameter, $FL\epsilon/\sqrt{K}$
$l_2$	length of plate downstream from the blocks [m]	$\mu$	dynamic viscosity [kg m <sup>-1</sup> s <sup>-1</sup> ]
$L$	length of the external boundary as shown in Fig. 1 [m]	$\nu$	kinematic viscosity [m <sup>2</sup> s <sup>-1</sup> ]
$n$	coordinate normal to the porous/fluid interface	$\xi$	vorticity
$N$	number of blocks	$\rho$	fluid density [kg m <sup>-3</sup> ]
$Nu$	Nusselt number, $hx/k_f$	$\Phi$	transported property; general dependent variable
$P$	pressure [Pa]	$\Psi$	stream function.
$Pe_L$	Peclet number, $u_x L/\alpha$	Superscript	
$Pr$	Prandtl number, $\nu/\alpha$	*	dimensionless quantity.
$Re_L$	Reynolds number, $u_x L/\nu$	Subscripts	
$t$	coordinate tangential to the porous/fluid interface	eff	effective
$T$	temperature [K]	f	fluid
$u$	$x$ -component velocity [m s <sup>-1</sup> ]	P	porous
$v$	$y$ -component velocity [m s <sup>-1</sup> ]	x	local
$\mathbf{v}$	velocity vector [m s <sup>-1</sup> ]	$\infty$	condition at infinity.
$W$	width of the porous block [m]	Other	
$x$	horizontal coordinate [m]	[a, b]	larger of a and b.

The main focus of this research is to analyze forced convection over a composite porous/fluid system composed of multiple porous blocks. Since very little work has been done on external forced convective flow and heat transfer in composite systems, the objective of the present work is to study the interaction phenomena occurring in the porous medium and the fluid layer. In addition, the effects of various parameters governing the physics of the problem under consideration are also analyzed. The results presented in this work will provide a valuable and fundamental framework for predicting heat transfer and fluid flow characteristics for other composite systems such as in electronic cooling and in heat exchanger design, heat transfer control or augmentation, drag reduction (as compared to the presence of solid blocks), some of the manufacturing processes, geothermal reservoirs and oil extraction. The present work constitutes one

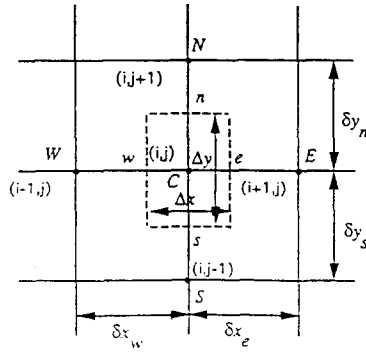
of the first analyses of the separated forced convection over porous blocks.

## THEORY

A schematic representation of the system under investigation is shown in Fig. 1. It consists of flow over a flat plate with multiple porous blocks attached on the external boundary. The height and width of the porous blocks are  $H$  and  $W$ , respectively, the distance between two blocks is  $D$ , the length of the wall is  $L$ , the free stream velocity is  $u_\infty$ , and the free stream temperature is  $T_\infty$ . The wall is maintained at constant temperature  $T_w$ . It is assumed that the flow is steady, laminar, incompressible, and two-dimensional. In addition, the thermophysical properties of the fluid and the porous matrix are assumed to be constant and the fluid-saturated porous media are



(a)



(b)

FIG. 1. (a) Schematic diagram of flow and heat transfer through a multiple porous block system. (b) Grid system for the computational domain.

considered homogeneous, isotropic and in local thermodynamic equilibrium with the fluid.

An efficient alternative method for combining the two sets of conservation equations for the fluid region and porous regions into one set of conservation equations is to model the porous substrate and the flow regions as a single domain governed by one set of conservation equations, the solution of which satisfies the continuity of the longitudinal and transverse velocities, normal and shear stresses, temperature, and the heat flux across the porous/fluid interface as described by the following equations (Sathe *et al.* [11]; Vafai and Kim [10]):

$$u_P|_{g(x,y)=0} = u_f|_{g(x,y)=0}, \quad v_P|_{g(x,y)=0} = v_f|_{g(x,y)=0} \tag{1a}$$

$$P_P|_{g(x,y)=0} = P_f|_{g(x,y)=0},$$

$$\mu_{eff} \frac{\partial v_P}{\partial n_P} \Big|_{g(x,y)=0} = \mu_f \frac{\partial v_f}{\partial n_f} \Big|_{g(x,y)=0} \tag{1b}$$

$$\mu_{eff} \left( \frac{\partial u_P}{\partial n_P} + \frac{\partial v_P}{\partial t_P} \right) \Big|_{g(x,y)=0} = \mu_f \left( \frac{\partial u_f}{\partial n_f} + \frac{\partial v_f}{\partial t_f} \right) \Big|_{g(x,y)=0} \tag{1c}$$

$$T_P|_{g(x,y)=0} = T_f|_{g(x,y)=0},$$

$$k_{eff} \frac{\partial T_P}{\partial n_P} \Big|_{g(x,y)=0} = k_f \frac{\partial T_f}{\partial n_f} \Big|_{g(x,y)=0} \tag{1d}$$

where  $g(x, y) = 0$  is the curve defining the porous/fluid interface. The derivative with respect to  $n$  and  $t$  rep-

resents the normal and tangential gradients, respectively, to the curve  $g(x, y) = 0$  at any point on the interface. In dimensionless form the above-mentioned equations governing the whole porous/fluid composite system can be written as (Vafai and Tien [12, 13])

$$\frac{\partial \Psi^*}{\partial y^*} \frac{\partial \xi^*}{\partial x^*} - \frac{\partial \Psi^*}{\partial x^*} \frac{\partial \xi^*}{\partial y^*} = \frac{1}{Re_L} \nabla^2 \xi^* + S^* \quad (2)$$

$$\nabla^2 \Psi^* = -\xi^* \quad (3)$$

$$\frac{\partial \Psi^*}{\partial y^*} \frac{\partial \theta}{\partial x^*} - \frac{\partial \Psi^*}{\partial x^*} \frac{\partial \theta}{\partial y^*} = \nabla \cdot \left( \frac{1}{Pe_L} \nabla \theta \right) \quad (4)$$

where  $(x^*, y^*)$  are dimensionless rectangular Cartesian coordinates and  $\Psi^*$  is the stream function which is related to the fluid velocity components  $u$  and  $v$  by

$$u = \frac{\partial \Psi}{\partial y}, \quad v = -\frac{\partial \Psi}{\partial x} \quad (5)$$

and  $\xi$  is the vorticity defined by

$$\xi = \frac{\partial v}{\partial x} - \frac{\partial u}{\partial y} \quad (6)$$

The non-dimensional parameters in the fluid region are

$$Re_L = \frac{u_x L}{\nu_f}, \quad Pe_L = \frac{u_x L}{\alpha_f}, \quad S^* = 0 \quad (7a)$$

and in the porous region the non-dimensional parameters are

$$Pe_L = \frac{u_x L}{\alpha_{eff}}, \quad Da_L = \frac{K}{L^2}, \quad \Lambda_L = \frac{FL\varepsilon}{K^{1/2}} \quad (7b)$$

$$S^* = -\frac{1}{Re_L Da_L} \xi^* - \Lambda_L |v^*| \xi^* - \Lambda_L \left( v^* \frac{\partial |v^*|}{\partial x^*} - u^* \frac{\partial |v^*|}{\partial y^*} \right) \quad (8)$$

The source term  $S^*$  can be considered as those contributing to the vorticity generation due to the presence of the porous medium. In addition, the dimensionless boundary conditions are

$$\Psi^* = y^*, \quad \xi^* = -\frac{\partial^2 \Psi^*}{\partial x^{*2}}, \quad \theta = 0, \quad \text{at } x^* = 0 \quad (9)$$

$$\Psi^* = 0, \quad \xi^* = -\frac{\partial^2 \Psi^*}{\partial y^{*2}}, \quad \theta = 1, \quad \text{at } y^* = 0 \quad (10)$$

$$\frac{\partial \Psi^*}{\partial y^*} = 1, \quad \xi^* = -\frac{\partial^2 \Psi^*}{\partial x^{*2}}, \quad \theta = 0, \quad \text{as } y^* \rightarrow \infty \quad (11)$$

$$\frac{\partial \Psi^*}{\partial x^*} = 0, \quad \frac{\partial \xi^*}{\partial x^*} = 0, \quad \frac{\partial \theta}{\partial x^*} = 0, \quad \text{as } x^* \rightarrow \infty \quad (12)$$

All of the above variables have been non-dimensionalized based on the following definitions

$$x^* = \frac{x}{L}, \quad y^* = \frac{y}{L}, \quad u^* = \frac{u}{u_x}, \quad v^* = \frac{v}{u_x}, \quad |v^*| = \sqrt{(u^{*2} + v^{*2})} \quad (13a)$$

$$\Psi^* = \frac{\Psi}{u_x L}, \quad \xi^* = \frac{L\Psi}{u_x}, \quad \theta = \frac{T - T_w}{T_w - T_x} \quad (13b)$$

It should be noted that these conservation equations for forced convection in porous media are developed here using the local volume-averaging technique (Vafai and Tien [12]). In addition, the conservation equations in porous media are also based on the generalized flow model, which take into account the effects of flow inertia as well as friction caused by macroscopic shear.

In this study, the problem is governed by seven parameters, i.e. the geometric parameters  $A = W^*/H^*$  and  $B = D^*/W^*$ ; Reynolds number,  $u_x L/\nu$ ; Darcy number,  $K/L^2$ ; inertia parameter,  $FL\varepsilon/\sqrt{K}$ ; the Prandtl number,  $\nu/\alpha$ ; and the number of blocks  $N$ . To evaluate the effects of the porous material on the shear stress and heat transfer rate at the wall, additional calculations were carried out. For the shear stress the results were cast in dimensionless form by means of the local friction coefficient as

$$C_{f,x} = \frac{\tau_{w,x}}{\rho u_x^2/2} = \frac{2}{Re_L} \frac{\partial u^*}{\partial y^*} \Big|_{y^*=0} \quad (14)$$

and for the heat transfer rate the results were represented in dimensionless form in terms of a dimensionless Nusselt number

$$Nu_x = \frac{hx}{k_f} = -x^* \frac{k_{eff}}{k_f} \frac{\partial \theta}{\partial y^*} \Big|_{y^*=0} \quad (15)$$

Note that the conductivity of the fluid was chosen in the formulation of the Nusselt number. This results in more meaningful comparisons for the heat flux at the external boundary between the composite system and the case where there was no porous substrate.

## NUMERICAL METHOD AND PROCEDURE

The fluid flow and heat transfer characteristics in the configuration of interest will be revealed after solving numerically the mathematical model outlined

in the previous section. The following is a general formulation for the diffusion–convection equation, which can be applied to vorticity, stream function, and temperature equations

$$\frac{\partial}{\partial x}(u\Phi) + \frac{\partial}{\partial y}(v\Phi) = \frac{\partial}{\partial x}\left(\Gamma\frac{\partial\Phi}{\partial x}\right) + \frac{\partial}{\partial y}\left(\Gamma\frac{\partial\Phi}{\partial y}\right) + S^* \quad (16)$$

Here  $\Phi$  represents any one of the pertinent variables. Based on a non-uniform rectangular grid system, the finite-difference form of equation (16) is derived by volume integration of the differential equation over discrete cells surrounding the grid points, as shown in Fig. 1(b). Application of central differencing for the diffusive term and the upwind differencing for the convective term gives

$$C_C\Phi_{i,j} = C_E\Phi_{i+1,j} + C_W\Phi_{i-1,j} + C_N\Phi_{i,j+1} + C_S\Phi_{i,j-1} + b \quad (17)$$

where

$$C_E = \Gamma_c \frac{\Delta y}{\delta x_c} (1 + [-\Gamma_c \delta x_c u_e, 0]) \quad (18a)$$

$$C_W = \Gamma_w \frac{\Delta y}{\delta x_w} (1 + [\Gamma_w \delta x_w u_w, 0]) \quad (18b)$$

$$C_N = \Gamma_n \frac{\Delta x}{\delta y_n} (1 + [-\Gamma_n \delta y_n v_n, 0]) \quad (18c)$$

$$C_S = \Gamma_s \frac{\Delta x}{\delta y_s} (1 + [\Gamma_s \delta y_s v_s, 0]) \quad (18d)$$

$$b = S^* \Delta x \Delta y \quad (18e)$$

and

$$C_C = C_E + C_W + C_N + C_S \quad (18f)$$

Applying the above discretization procedure for vorticity, stream function, and temperature equations gives

$$C_C \xi_{i,j}^* = C_E \xi_{i+1,j}^* + C_W \xi_{i-1,j}^* + C_N \xi_{i,j+1}^* + C_S \xi_{i,j-1}^* + S^* \Delta x \Delta y \quad (19)$$

$$C_C \Psi_{i,j}^* = C_E \Psi_{i+1,j}^* + C_W \Psi_{i-1,j}^* + C_N \Psi_{i,j+1}^* + C_S \Psi_{i,j-1}^* + \xi^* \Delta x \Delta y \quad (20)$$

$$C_C \theta_{i,j} = C_E \theta_{i+1,j} + C_W \theta_{i-1,j} + C_N \theta_{i,j+1} + C_S \theta_{i,j-1} \quad (21)$$

Equations (19)–(21) give a system of linear equations for  $\xi^*$ ,  $\Psi^*$ , and  $\theta$ . These finite-difference equations were solved by the extrapolated-Jacobi scheme—an iterative scheme based on a double cyclic routine—which translates into a sweep of only half of the grid points at each iteration step (Adams and Ortega [14]). It was necessary to use underrelaxation to prevent instability and divergence due to nonlinearity in these finite-difference equations. The numerical integration

was performed until the following convergence criterion was satisfied

$$\max \left| \frac{\phi_{i,j}^{n+1} - \phi_{i,j}^n}{\phi_{i,j}^n} \right| < 10^{-6} \quad (22)$$

where  $\phi$  stands for  $\xi^*$ ,  $\Psi^*$ , or  $\theta$  and  $n$  denotes the iteration number.

A non-uniform grid system, which possesses a very fine grid structure through the porous block array as well as its immediate surroundings and gradually becomes coarser towards the far field, was employed. A grid independence test for  $Re_L = 3 \times 10^5$ ,  $Da_L = 8 \times 10^{-6}$ ,  $\Lambda_L = 0.35$ ,  $Pr = 0.7$ ,  $A = 6$ ,  $B = 1$ , and  $N = 4$  showed that there is only a very small difference (less than 1%) in the streamlines and isotherms among the solutions for  $82 \times 82$ ,  $144 \times 162$ , and  $172 \times 202$  grid distributions. As this difference is small, all of our computations were based on the  $144 \times 162$  grid system. It was found that any further increase in the grid distribution resulted less than 1% difference for cases studied in this work.

To accommodate the simultaneous solutions of the transport equations in both fluid and porous regions, the effective viscosity of the fluid-saturated porous medium is set to be equal to the viscosity of the fluid. It has been found that this approximation provides good agreement with experimental data (Vafai and Thiyagaraja [7]; Neale and Nader [15]). Moreover, the dimensionless groups  $\Lambda_L$  and  $Da_L$  at the interface of a control volume are computed by the harmonic mean.

The interface between the porous medium and fluid space requires special consideration. This is due to the sharp change of thermophysical properties, such as the permeability, porosity, and the thermal conductivity, across the interface. All of these effects on the porous/fluid interface are summarized in the dimensional parameters  $Da_L$ ,  $\Lambda_L$  and  $Pr$ . The harmonic mean formulation suggested by Patankar [16] was used to handle these discontinuous characteristics in the porous/fluid interface. For the present case,  $Da_L$ ,  $\Lambda_L$  and  $Pr$  at the interface of a control volume are as follows

$$Da_{L_i} = \frac{2Da_{L_{eff}}Da_{L_f}}{Da_{L_{eff}} + Da_{L_f}}, \quad \Lambda_{L_i} = \frac{2\Lambda_{L_{eff}}\Lambda_{L_f}}{\Lambda_{L_{eff}} + \Lambda_{L_f}}, \quad Pr_i = \frac{2Pr_{eff}Pr_f}{Pr_{eff} + Pr_f} \quad (23)$$

where the subscripts eff, f, and I stand for effective, fluid, and interfacial, respectively. Therefore, instead of the source terms in equations (7a) and (8), the following source terms were used across the interface

$$S^* = \frac{u^*}{Re_L} \frac{\partial}{\partial y^*} \left( \frac{1}{Da_\Lambda} \right) - \frac{v^*}{Re_L} \frac{\partial}{\partial x^*} \left( \frac{1}{Da_\Lambda} \right) + |v^*|u^* \frac{\partial}{\partial y^*} (\Lambda_L) - |v^*|v^* \frac{\partial}{\partial x^*} (\Lambda_L) \quad (24)$$

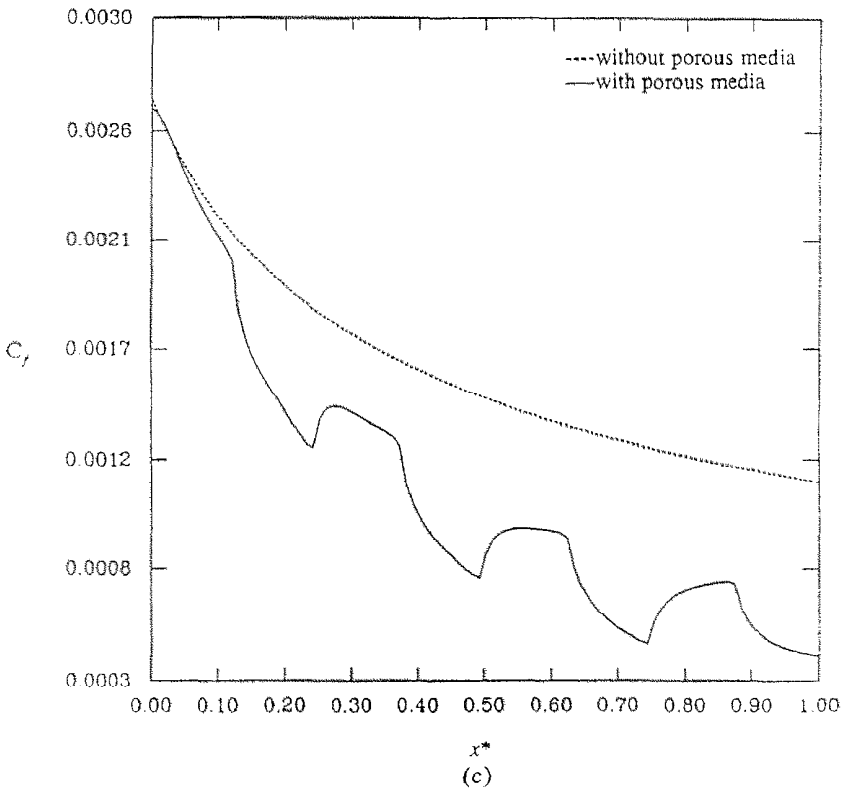
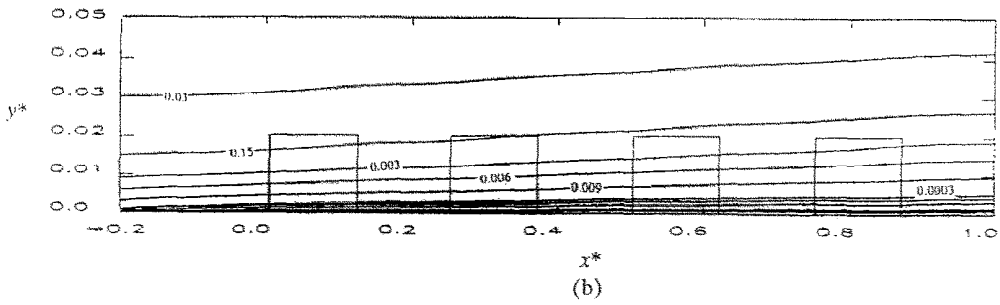
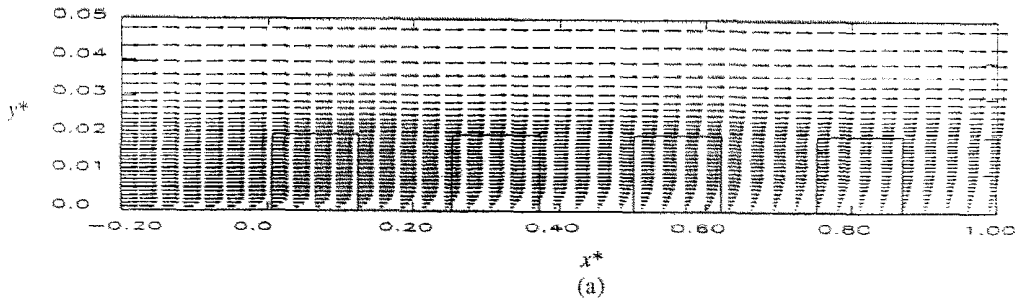


FIG. 2. (a) Velocity distribution, (b) streamlines, and (c) frictional coefficient for flow through four obstructing porous blocks for  $Re_L = 3 \times 10^5$ ,  $Da_L = 8 \times 10^{-6}$ ,  $\Lambda_L = 0.35$ ,  $A = 6$ ,  $B = 1$ ,  $H^* = 0.02$ .

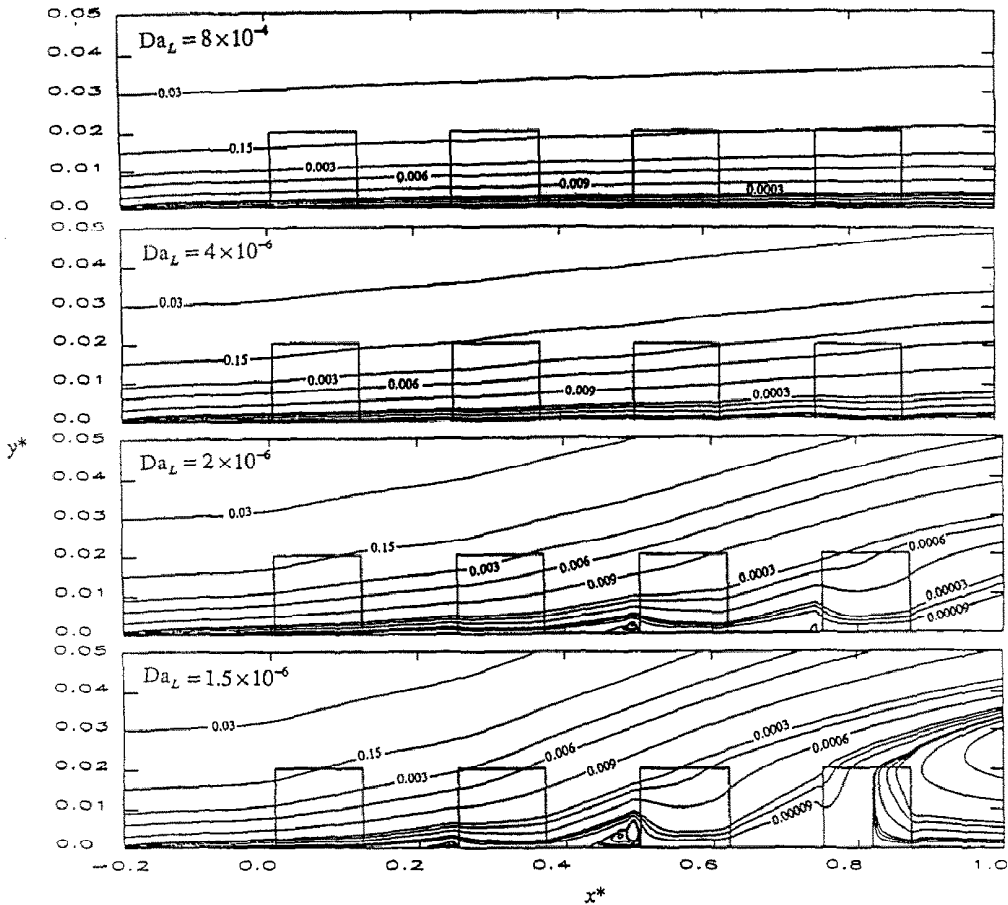


Fig. 3. Effects of the Darcy number on streamlines for flow through four obstructing porous blocks for  $Re_L = 3 \times 10^5$ ,  $\Lambda_L = 0.35$ ,  $A = 6$ ,  $B = 1$ ,  $H^* = 0.02$ .

$$\begin{aligned}
 S^* = & -\frac{1}{Re_L Da_L} \xi^* - \Lambda_L |v^*| \xi^* \\
 & - \Lambda_L \left( v^* \frac{\partial |v^*|}{\partial x^*} - u^* \frac{\partial |v^*|}{\partial y^*} \right) \\
 & + \frac{u^*}{Re_L} \frac{\partial}{\partial y^*} \left( \frac{1}{Da_L} \right) - \frac{v^*}{Re_L} \frac{\partial}{\partial x^*} \left( \frac{1}{Da_L} \right) \\
 & + |v^*| u^* \frac{\partial}{\partial y^*} (\Lambda_L) - |v^*| v^* \frac{\partial}{\partial x^*} (\Lambda_L) \quad (25)
 \end{aligned}$$

where equation (24) was used for the fluid and equation (25) was used for the porous region. Note that constant values of  $Da_L$ , and  $\Lambda_L$  were used for a specified porous substrate.

In our investigation the computational domain is chosen to be larger than the physical domain. Along the  $x$ -direction, the computational domain starts at a distance of one-fifth of total length upstream of the physical domain. This procedure eliminates the errors associated with the singular point at the leading edge of the composite system. On the other side, the computational domain is extended over a distance of two-

fifths of the total length downstream from the trailing edge of the physical domain. Since the present problem has a significant parabolic character, the downstream boundary condition on the computational domain does not have much influence on the physical domain. In the  $y$ -direction the length of the computational domain was systematically increased until the maximum vorticity changes for two consecutive runs became less than 1%.

In order to examine the validity of the present numerical model, comparisons with more classical results were made. They were performed for laminar flow over a flat plate (i.e.  $H^* = 0$ , no porous substrate) and that over a flat plate embedded in a porous medium (i.e.  $H^* \rightarrow \infty$  and  $W^* \rightarrow \infty$ , full porous medium). The results for  $H^* = 0$  agree to better than 1% with boundary layer similarity solutions for velocity and temperature fields. The results for  $H^* \rightarrow \infty$  and  $W^* \rightarrow \infty$  agree extremely well with data reported by Vafai and Thiyagaraja [7]. These comparisons were found to be similar to those presented in Vafai and Kim [10].

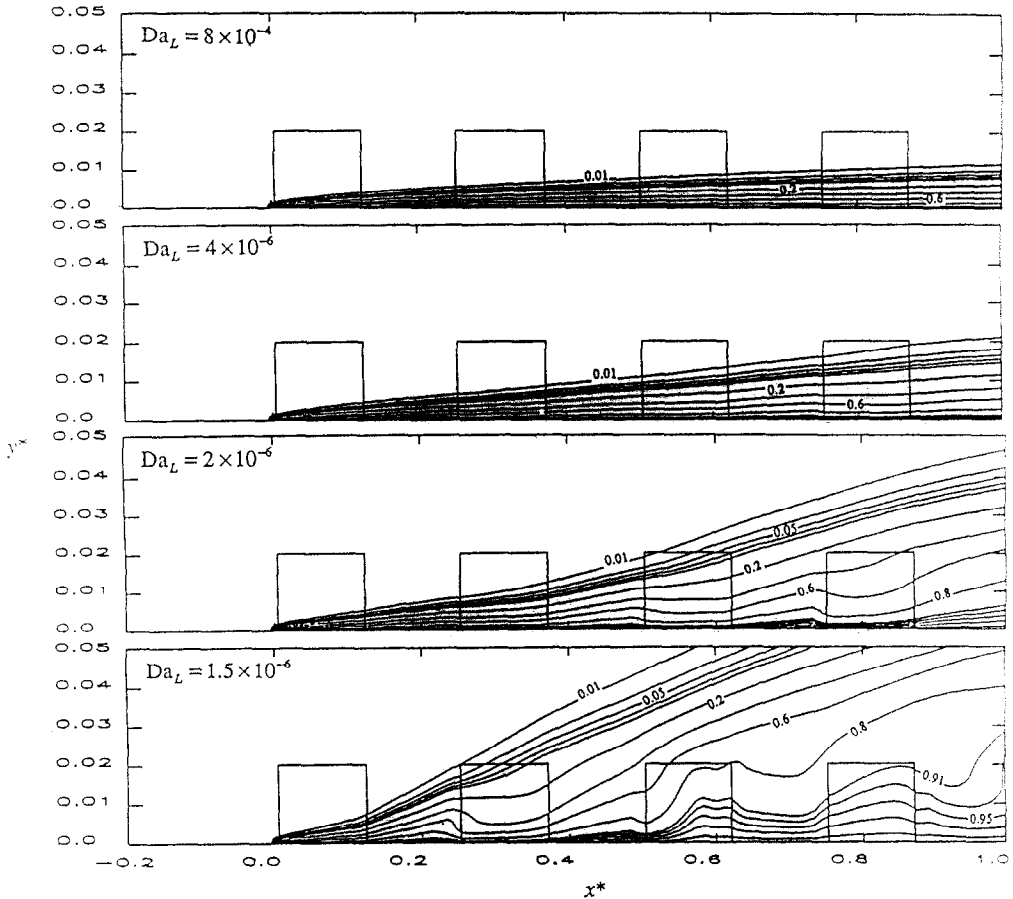


Fig. 4. Effects of the Darcy number on isotherms for flow through four obstructing porous blocks for  $Re_L = 3 \times 10^5$ ,  $\Lambda_L = 0.35$ ,  $Pr = 0.7$ ,  $k_{eff}/k_f = 1.0$ ,  $A = 6$ ,  $B = 1$ ,  $H^* = 0.02$ .

## RESULTS AND DISCUSSION

The effects of governing physical parameters, such as the Reynolds number, Darcy number, Prandtl number, and inertial parameter, as well as the geometric arrangements of the porous block array on the flow and temperature fields were explored. To illustrate the results of the flow and temperature fields, only the portion which concentrates on the porous block array and its close vicinity is presented. However, the much larger domain was always used for numerical calculations and interpretation of the results. It should be noted that for the sake of brevity, the main features and characteristics of some of the results are only discussed and the corresponding figures are not presented.

The influences of the porous block array on the velocity field is depicted in Fig. 2(a) for a case where the Reynolds number is  $3 \times 10^5$ , the Darcy number is  $8 \times 10^{-6}$ , the inertial number is 0.35, the dimensionless height and width of the porous block are 0.02 and 0.12, respectively, and the spacing between the porous blocks is 0.12. It can be seen that there are two distinct

momentum boundary layers in the flow field. One is along the impermeable wall and the other is along the top of porous obstacles. Inside the porous media as the normal coordinate increases the velocity distribution increases from zero to a constant value, which is maintained until the outer boundary layer appears. The velocity distribution goes through a smooth transition once it crosses the porous/fluid interface, and finally approaches a free-stream value. As expected, both momentum boundary layers grow in the streamwise coordinate. Consequently, in the porous region the magnitude of the interfacial velocity between these two boundary layers decreases to adapt this growth, resulting in further increase in the thickness of the boundary layer near the wall. Inside of the inter-block spacing, the flow is decelerated and is eventually forced to reverse its direction near the wall, resulting in a boundary layer separation. This is due to the adverse pressure caused by the porous obstacle.

The above-described flow field can also be observed by streamlines shown in Fig. 2(b). It can be observed that the streamlines move upward due to the presence of the porous blocks. This indicates that the flow is

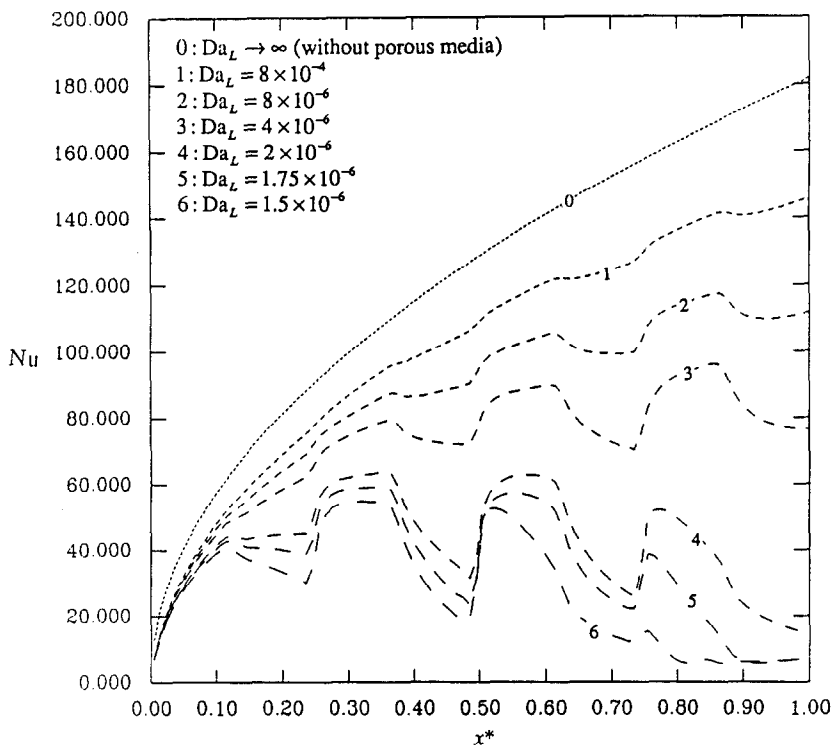


FIG. 5. Effects of the Darcy number on the Nusselt number for flow through four obstructing porous blocks for  $Re_L = 3 \times 10^5$ ,  $\Lambda_L = 0.35$ ,  $Pr = 0.7$ ,  $k_{eff}/k_f = 1.0$ ,  $A = 6$ ,  $B = 1$ ,  $H^* = 0.02$ .

directed upwards periodically while encountering the porous blocks. This effect is more pronounced for smaller Darcy numbers or larger inertial parameters. This phenomenon is due to the relatively larger resistance that the flow encounters inside the porous blocks, which in turn displaces the fluid by blowing it from the porous region into the fluid region. These results were also found in the work of Vafai and Kim [10]. The flow patterns, including the shape of boundary layer and the blowing effect from porous blocks, play an important role in affecting the temperature distribution. Figure 2(c) displays the periodical streamwise variation of the local friction coefficient at the wall. It can be seen that the friction coefficient decreases with an increase of the boundary layer thickness and increases with a decrease in the boundary layer thickness. This is the reason for the fluctuation of the local friction coefficient along the external boundary. It can be seen that inside the porous medium the friction at the wall decreases. This decrease is a direct result of the blowing effect, as discussed previously. However, in the space between the porous blocks the adverse pressure caused by porous obstacle reduces the fluid momentum resulting in a rapid increase in the boundary layer thickness. Consequently, the friction coefficient significantly decreases in the inter-block spacings.

#### Effects of the Darcy number

The Darcy number is directly related to the permeability of the porous medium. To investigate the

effect of Darcy number on the flow and temperature fields, computations were carried out at  $Da_L = 8 \times 10^{-4}$ ,  $4 \times 10^{-6}$ ,  $2 \times 10^{-6}$ , and  $1.5 \times 10^{-6}$  for  $H/L = 0.02$ ,  $A = 6$ ,  $B = 1$ ,  $Re_L = 3 \times 10^5$  and  $\Lambda_L = 0.35$ . Results of the computations for streamlines, isotherms, and local Nusselt numbers are presented in Figs. 3–5. It can be seen from Fig. 3 that by decreasing the Darcy number up to a certain value (less than  $4 \times 10^{-6}$ ) the boundary layer starts to separate from a certain location at the wall, and then forms a separation region along the streamwise direction near the wall. The size of separation region increases in the inter-block spacing due to the adverse pressure gradient caused by porous obstacles, and decreases inside the porous media due to the bulk frictional resistance offered by the porous matrix. The appearance of a vortex zone depends on whether the flow reattaches the wall or not. Outside the boundary layer flow the blowing effect caused by porous media increases as the Darcy number decreases, which leads to the larger upward moving of the streamlines and the reduction of the mass flow rate passing through the porous media. The closely spaced streamlines indicate that there are larger volume flow rates. The temperature fields shown in Fig. 4 correspond to a case where the Prandtl number is 0.7 and the conductivity of the porous media is equal to that of the fluid. A smaller value of  $Da_L$  translates into larger blowing effects which divert the flow through the porous medium. Therefore, as the Darcy number decreases, the thickness of the thermal boundary layer increases

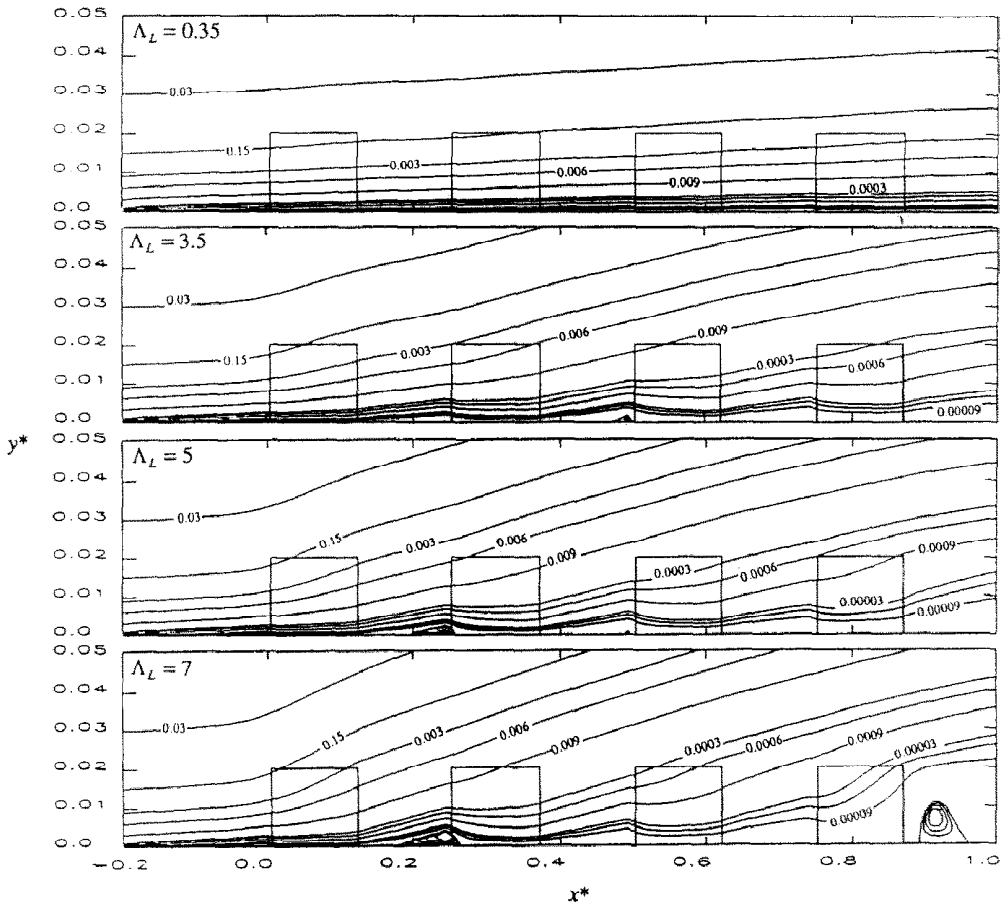


FIG. 6. Effects of the inertial parameter on streamlines for flow through four obstructing porous blocks for  $Re_L = 3 \times 10^5$ ,  $Da_L = 8 \times 10^{-6}$ ,  $A = 6$ ,  $B = 1$ ,  $H^* = 0.02$ .

and the distortion of isotherm near the wall becomes more noticeable. The increase in the distortion of the isotherms at lower values of  $Da_L$  is due to the presence of a larger fluctuating separation zone near the wall. The fluctuations in the momentum and thermal boundary layers also create the oscillations in the local Nusselt number distribution as depicted in Fig. 5. It is seen that the Darcy number has a significant impact on the local Nusselt number distribution. The local Nusselt number fluctuates periodically as the stream-wise coordinate increases due to the presence of the porous blocks, with an increasing mean at the higher Darcy numbers (higher than  $2 \times 10^{-6}$ ) and a decreasing mean at the lower Darcy numbers. Moreover, the extent of the fluctuation increases for lower values of Darcy numbers. The trough in each cycle occurs at an  $x^*$  value corresponding to the left face of each porous block. This is due to the slow circulating motion inside the separating zones in front of the porous obstacles, resulting in low heat transfer rates in these regions. In particular, for the lower Darcy number heat transfer in circulating regions decreases due to the larger size of separation zone. It should be noted that flow and heat transfer characteristics for the configuration shown in Fig. 1 are entirely different than flow and

heat transfer characteristics for forced convection over intermittently placed porous cavities [17].

#### *Inertial effects*

When the Reynolds number based on the pore diameter becomes large the inertial effects become significant. The effects of an increase or decrease in the inertial parameter are shown in Figs. 6 and 7, for  $Re_L = 3 \times 10^5$ ,  $Da_L = 8 \times 10^{-6}$ ,  $Pr = 0.7$ ,  $A = 6$ , and  $B = 1$  at  $\Lambda_L = 0.35, 3.5, 5$ , and  $7$ , respectively. Comparison of the streamlines in Fig. 6 shows that as the inertial parameter increases, the distortion of streamlines becomes more significant and the size of the vortices near the wall increases. This is because of the larger bulk frictional resistance that the flow experiences for larger inertial parameters. Therefore, larger values of  $\Lambda_L$  would lead to a larger blowing effect thus reducing the mass flow rate through the porous blocks. In addition, the larger bulk frictional resistance caused by the porous matrix results in a larger adverse pressure gradient in front of the porous obstacle. As a result, the flow near the wall is decelerated more quickly and is eventually forced to reverse its direction forming a larger separation zone. When

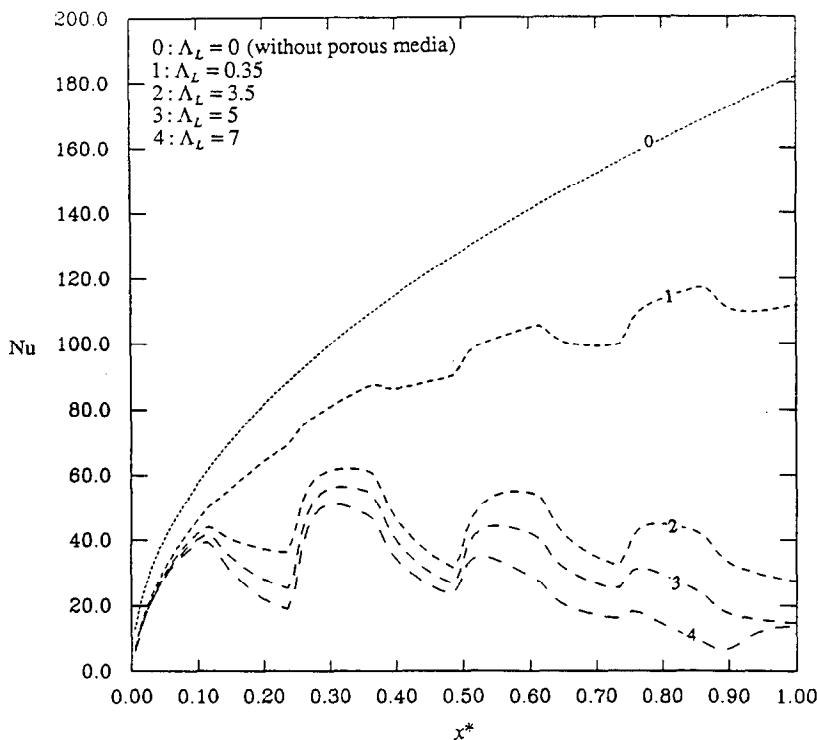


FIG. 7. Effects of the inertial parameter on the Nusselt number for flow through four obstructing porous blocks for  $Re_L = 3 \times 10^5$ ,  $Da_L = 8 \times 10^{-6}$ ,  $Pr = 0.7$ ,  $k_{eff}/k_f = 1.0$ ,  $A = 6$ ,  $B = 1$ ,  $H^* = 0.02$ .

entering the porous block, the laminar eddies in the separation zone are weakened by the frictional resistance of the porous matrix. This results in the reattachment of the boundary layer to the wall, and formation of a closed vortex region. Comparison of the isotherms shows that the larger the value of  $\Lambda_L$ , the larger the thickness of the thermal boundary layer, and the more noticeable the distortion of the isotherms. The reason for this behavior is similar to the effect of Darcy number on the temperature field. As in the case of Darcy number variations, a periodic variation of local Nusselt number is observed. As can be seen in Fig. 7 for smaller inertial parameters the mean value of the Nusselt number increases while for larger inertial parameters the mean value of the Nusselt number decreases with the flow direction. This shows that the inertial parameter has a significant effect on the formation and the size of the separation vortex and the convective energy transport.

#### Effects of Reynolds number

Figures 8 and 9 show streamlines and Nusselt number distribution for  $Da_L = 8 \times 10^{-6}$ ,  $\Lambda_L = 0.35$ ,  $Pr = 0.7$ ,  $A = 6$ , and  $B = 1$  with  $Re_L = 3 \times 10^5$ ,  $2 \times 10^5$ ,  $1.5 \times 10^5$  and  $1 \times 10^5$ , respectively. As expected, distortions in the streamlines and boundary layer thickness become evident as the Reynolds number decreases (see Fig. 8). The reason for this trend is that the lower the Reynolds number, the lower the flow inertia, thus reducing the extent of penetration

of the flow into the porous blocks. This results in a larger blowing effect in the flow field, and a larger thickness of boundary layer near the wall. Comparison of the temperature fields corresponding to different Reynolds numbers shows that for the lower Reynolds number the heat is transferred further out into the flow field. The variation of the local Nusselt number is shown in Fig. 9 with a different increasing mean for different Reynolds number. As expected, the heat transfer rate from the wall decreases with a decrease in the Reynolds number. This obviously is due to lower velocities near the wall for smaller Reynolds numbers. It is this decrease in the transfer of convective energy that causes a lower temperature gradient and heat flux at the wall. As with the other two cases, a periodic variation of local Nusselt number is again observed.

#### Prandtl number effects

To investigate the effect of the Prandtl number on the flow and temperature fields, three different Prandtl numbers were chosen such that they will cover a wide range of thermophysical fluid properties. The numerical results are presented in Fig. 10 at  $Re_L = 3 \times 10^5$ ,  $Da_L = 8 \times 10^{-6}$ ,  $\Lambda_L = 0.35$ ,  $A = 6$ , and  $B = 1$  for three different fluids with  $Pr = 0.7$  (air),  $Pr = 7$  (water), and  $Pr = 100$  (a representative oil), respectively. Obviously, the Prandtl number variations have no effect on the flow field and the velocity distribution will be exactly the same as that shown in Fig. 2(a).

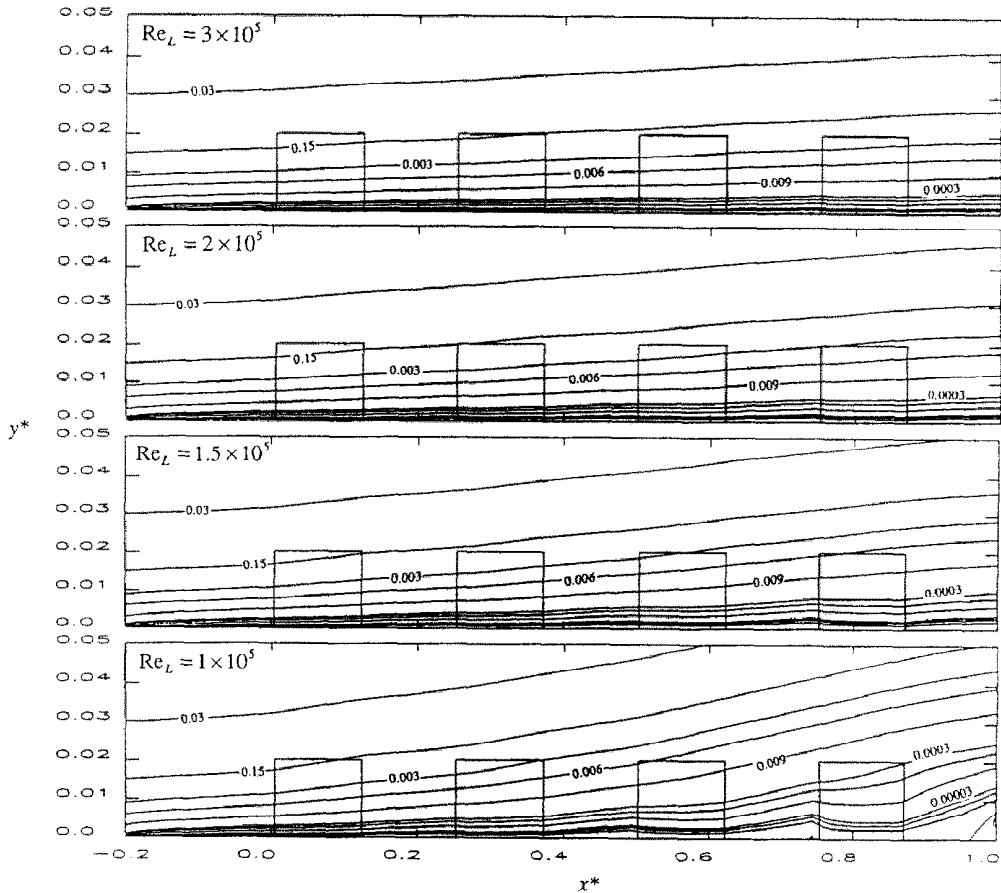


FIG. 8. Effects of the Reynolds number on streamlines for flow through four obstructing porous blocks for  $Da_i = 8 \times 10^{-6}$ ,  $\Lambda_L = 0.35$ ,  $A = 6$ ,  $B = 1$ ,  $H^* = 0.02$ .

Due to the lower value of the thermal diffusivity the temperature gradient is larger for larger Prandtl numbers. As expected, the local Nusselt number and its fluctuations increases with an increase in the Prandtl number, as shown in Fig. 10.

#### *Effects of the geometric parameters A and B*

When the value of  $A$ , related to the aspect ratio, was decreased, the distortions of streamlines and isotherms becomes less pronounced, and the closed vortex zones along the wall disappear. This is the direct result of reduction in the aspect ratio which lessens the blowing action and subsequent deceleration of the flow field. The second geometric parameter  $B = D^*/W^*$  reflects the influence of the inter-block spacing. It was found that as the inter-block spacing decreases, streamline and isotherm distortions become more pronounced. However, for lower values of  $B$ , the inter-block separation zones along the wall is reduced, while a larger separation zone forms behind the last block. This is because the smaller inter-block spacing weakens deceleration action on the boundary layer thus reducing the extent of the separation zone within that space. Also, the effects of additional number of blocks were

investigated. It was found that the increase in the number of blocks has no effect on the main features of the flow and temperature fields.

#### CONCLUSIONS

The flow field and thermal characteristics of external laminar forced convection flow over a porous block array are investigated numerically. Computations for flow and temperature fields were performed to study the effects of various governing parameters, such as Reynolds number, Darcy number, inertial parameter, Prandtl number and two geometric parameters. Comparisons of the local Nusselt number at the wall with and without porous promoters were also made. Two distinct boundary layers were shown to exist for the velocity field, while only one boundary layer was observed for the temperature field. It was shown that the porous block array significantly reduces the heat transfer rate at the wall. The extent of the reduction depends on the values of the governing parameters. The variation of local Nusselt number distribution with an increasing or decreasing mean is determined by whether or not there is the isolated

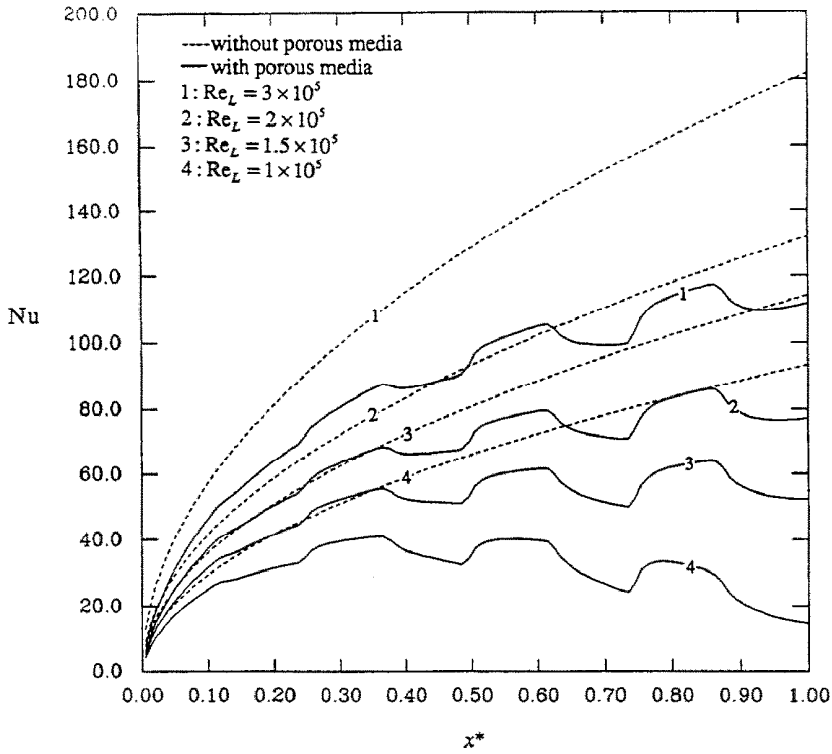


FIG. 9. Effects of the Reynolds number on the Nusselt number for flow through four obstructing porous blocks for  $Da_L = 8 \times 10^{-6}$ ,  $\Lambda_L = 0.35$ ,  $Pr = 0.7$ ,  $k_{eff}/k_f = 1.0$ ,  $A = 6$ ,  $B = 1$ ,  $H^* = 0.02$ .

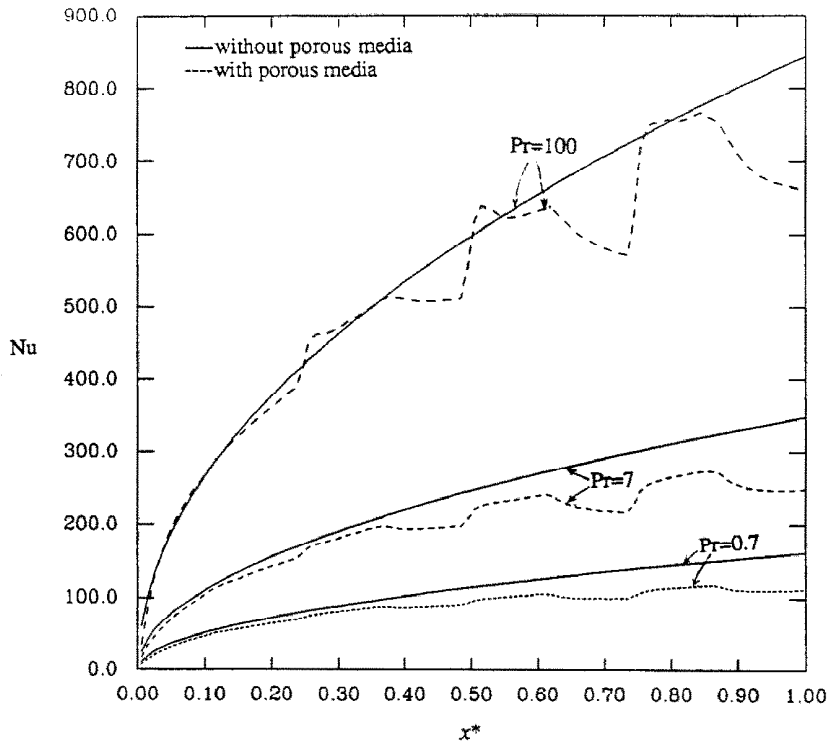


FIG. 10. Effects of the Prandtl number on the Nusselt number for flow through four obstructing porous blocks for  $Re_L = 3 \times 10^5$ ,  $Da_L = 8 \times 10^{-6}$ ,  $\Lambda_L = 0.35$ ,  $k_{eff}/k_f = 1.0$ ,  $A = 6$ ,  $B = 1$ ,  $H^* = 0.02$ .

vortex flow near the wall. Therefore, this configuration can be used as a thermal insulator for flows which have strong parabolic characters. Overall, it is shown that the presence of a porous block array near an impermeable boundary significantly changes the convection characteristics.

*Acknowledgement*—The grant from the Ohio Supercomputer Center is acknowledged and appreciated.

#### REFERENCES

1. A. D. Gosman, The TEACH-T computer program structure, flow, heat and mass transfer in turbulent recirculating flows—prediction and measurement, Lecture Notes from McGill University, Canada (1976).
2. A. M. Gooray, C. B. Watkins and W. Aung, Numerical calculations of turbulent heat transfer downstream of a rearward-facing step, *Proc. 2nd Int. Conf. Numer. Meth. Laminar Turbulent Flow*, Venice, Italy, pp. 639–651 (1981).
3. A. M. Gooray, C. B. Watkins and W. Aung,  $K-\epsilon$  calculations of heat transfer in redeveloping turbulent boundary layers downstream of reattachment. Presented at AIAA/ASME Thermophysics Conf., St Louis, MO, 6–9 June, ASME Paper No. 82-HT-77 (1982).
4. P. Cheng, Combined free and forced convection flow about inclined surfaces in porous media, *Int. J. Heat Mass Transfer* **20**, 807–814 (1977).
5. A. Bejan, *Convection Heat Transfer*. Wiley, New York (1984).
6. M. Kaviany, Boundary layer treatment of forced convection heat transfer from a semi-infinite flat plate embedded in porous media, *ASME J. Heat Transfer* **109**, 345–349 (1987).
7. K. Vafai and R. Thiyagaraja, Analysis of flow and heat transfer at the interface region of a porous medium, *Int. J. Heat Mass Transfer* **30**, 1391–1405 (1987).
8. P. Cheng, Mixed convection about a horizontal cylinder and a sphere in a saturated porous medium, *Int. J. Heat Mass Transfer* **25**, 1245–1247 (1982).
9. P. Cheng and T. M. Zheng, Thermal dispersion effects in forced convection plume above a horizontal line source of heat in a packed bed, *Int. J. Heat Mass Transfer Commun.* (1985).
10. K. Vafai and S. J. Kim, Analysis of surface enhancement by a porous substrate, *ASME J. Heat Transfer* **112**, 700–705 (1990).
11. S. B. Sathe, W. Q. Lin and T. W. Tong, Natural convection in enclosures containing an insulation with a permeable fluid-porous interface, *Int. J. Heat Fluid Flow* **9**, 389–395 (1988).
12. K. Vafai and C. L. Tien, Boundary and inertia effects on flow and heat transfer in porous media, *Int. J. Heat Mass Transfer* **24**, 195–203 (1981).
13. K. Vafai and C. L. Tien, Boundary and inertia effects on convective mass transfer in porous media, *Int. J. Heat Mass Transfer* **25**, 1183–1190 (1982).
14. J. Adams and J. Ortega, A multicolor SOR method for parallel computation, *Proc. Int. Conf. Parallel Procession* 53–56 (1982).
15. G. Neale and W. Nader, Practical significance of Brinkman's extension of Darcy's law: coupled parallel flows within a channel and a bounding porous medium, *Can. J. Chem. Engng* **52**, 475–478 (1974).
16. S. V. Patankar, *Numerical Heat Transfer and Fluid Flow*. Hemisphere, Washington, D.C. (1980).
17. K. Vafai and P. C. Huang, Analysis of heat transfer regulation and modification employing intermittently emplaced porous cavities, to appear in *ASME J. Heat Transfer*.